# DEM-CFD simulation of a dense fluidized bed: wall boundary and particle size effects

# DEM-CFD simulation of a dense fluidized bed: wall boundary and particle size effects

Prashant Gupta[1,*], J. Sun[*], J.Y. Ooi[*]

*School of Engineering, University of Edinburgh, Edinburgh, EH9 3JL, UK*

**Abstract**

We simulate a small-scale dense gas-solid fluidized bed using an approach coupling the averaged Navier-Stokes equation with a discrete description of particle dynamics. The simulation results are compared to the voidage, solid velocity and granular temperature measured using magnetic resonance (MR) and other experimental measurements for the same fluidized bed. It is found that the simulation is able to predict the minimum fluidization velocity and pressure drop with reasonable agreement and qualitatively capture the solid circulation pattern to a similar degree achieved by previous such simulations. The discrepancies for the solid velocities near the walls and in the central region at upper and lower bed heights were investigated by examining various models of the physical system and the sensitivity of the simulation results to these models. We demonstrate that the particle–wall interaction dominates the particle dynamics in a boundary layer of about 5 particle diameters to the wall and that modelling the wall using fixed particle of comparable size to the fluidized particles provides enhanced resistance reducing solid wall-slip velocity and granular temperature at the boundary layer. Modelling of particle size is shown to be important for capturing the variation of bed dynamics along the bed height direction.

*Keywords:* DEM-CFD, Fluidization, PARDEM, Particle–wall interaction

[*]Corresponding author

*Email addresses:* Now at Newcastle University
prashant.gupta@newcastle.ac.uk (Prashant Gupta), j.sun@ed.ac.uk (J. Sun), j.ooi@ed.ac.uk (J.Y. Ooi)

## 1. Introduction

Gas-solid fluidization is a critical process to many industrial operations, such as those in chemical and pharmaceutical industries, owing to the high rates of mass and heat transfer between the interacting phases. Design, optimization and scaling-up of such processes require a better understanding of the bed hydrodynamics, which is determined by the particle-level interactions between fluid, particle and boundaries. This understanding can be enhanced by using reliable numerical simulations [1], which provide dynamic data at locations and spatial or temporal scales complementary to those obtained using experimental techniques.

Recent advancements in physical models, numerical method and computer algorithm have enabled simulations of fluidization dynamics at different levels of details and the development of multiscale models linking these levels in a single simulation (e.g., as reviewed in [1]). One such multiscale model couples an averaged Navier-Stokes equation for the fluid phase with a discrete method solving for motion of individual particles. These type of models are able to capture the discrete nature of the particle phase while maintaining the computational tractability by not solving the detailed fluid field at the particle level. These have been generally known as coupling between computational fluid dynamics (CFD) and discrete element method (DEM) [2], although other names, such as discrete particle models [3], have been used for essentially the same methodology. The general theoretical framework has been established (with details reviewed in [2]) for DEM-CFD models, which have been shown to be able to capture various fluidization phenomena qualitatively. For example, the simulations and comparisons with 2-dimensional images from experiments for single bubble dynamics and segregation of binary mixtures have been reviewed in [3] and [4], respectively.

The effort to more quantitatively validate DEM-CFD models and codes have been revived in recent years upon the availability of experimental data of bed dynamics at higher spatial and temporal resolutions in 3D. Such data have been obtained using non-invasive experimental techniques such as positron emission particle tracking (PEPT) [5] and magnetic resonance (MR) measurements [6]. Using MR techniques, Müller et al. [7, 8] measured voidage, solid velocity and granular temperature for a thin gas-solid fluidized bed with spatial resolutions comparable to the size of the fluidized particles. Such data have been used to validate various DEM-CFD codes [7, 8, 9]. These studies have shown similar DEM-CFD predictions and claimed to

have captured qualitatively fluidization dynamics. However, when compared quantitatively, large discrepancies have been identified. Generally speaking the near-wall solid velocity [7, 9] and granular temperature [7] were over-predicted; the central solid velocities [7, 9] were over- and under-predicted at the lower and upper bed regions, respectively. Their parametric studies showed that the simulation results were not sensitive to particle stiffness, rolling friction coefficient, particle–wall friction coefficient [9], particle coefficients of restitution and friction [8], or different fluid–particle drag models [7]. Higher particle–wall friction coefficient was found to improve slightly the solid velocity predictions near the walls [7, 9]. However, no further improvement was observed for the friction coefficients higher than 0.3 [9]. Taking into account non-sphericity in the drag model of Gidaspow [10] only increased the solid velocities throughout the bed height [9]. The questions regarding the causes of the discrepancies and how to address them in a DEM-CFD framework therefore remain open.

In this paper we focus on addressing these questions by studying the same fluidized bed as in the MR experiments [7, 8] using DEM-CFD simulations. The methodology of the DEM-CFD models is similar to others, but has a slightly different numerical implementation [11] discussed in the next section. We obtain similar simulation results when using the same models and parameters as before [7, 8, 9]. It is examined that how particle dynamics near the walls is effected by the particle–wall interaction. These are modelled by interaction of fluidized DEM particles with the fixed particles of comparable sizes, rather than using a planar frictional wall. The effect of the wall boundaries using the fixed particles is checked for both the solid velocity and the granular temperature predictions near the walls. Furthermore, effects of particle size on the bed expansion and dynamics are examined so as to explain the over- and under-predictions of solid velocity in the central region found from the base simulations.

## 2. Governing equations and closure models

In the DEM-CFD methodology, the fluid velocity at each point in space is replaced by its average, taken over a spatial domain large enough to contain many particles but still small compared to the whole region occupied by the flowing mixture. Newtonian equations of motion are solved for each particle in a Lagrangian framework. The coupling force between fluid and particles is then related to the particles velocity relative to the locally averaged fluid ve-

locity and to the local concentration of the particle assembly. The equations for the gas, particles and inter-phase coupling are presented as follows.

*2.1. Gas phase equations*

The locally averaged incompressible continuity and momentum equations for the gas phase [12, 13] are given by

$$\frac{\partial \epsilon}{\partial t} + \boldsymbol{\nabla} \cdot (\epsilon \mathbf{u}_f) = 0, \tag{1}$$

and

$$\rho_f \frac{\partial \epsilon \mathbf{u}_f}{\partial t} + \rho_f \nabla \cdot (\epsilon \mathbf{u}_f \mathbf{u}_f) = -\boldsymbol{\nabla} p + \boldsymbol{\nabla} \cdot \tau_f + \epsilon \rho_f \mathbf{g} - \mathbf{I}_f, \tag{2}$$

where $\epsilon$ is the porosity; $\mathbf{u}_f$, $p$, $\rho_f$ and $\tau_f$ are the fluid velocity, pressure, density and viscous stress tensor respectively; $\mathbf{g}$ is the gravitational acceleration; and $\mathbf{I}_f$ is the inter-phase momentum transfer term arising due to fluid–particle interactions. It is noted here that bold symbols indicate vectors.

*2.2. Discrete element method*

Each particle's motion is solved using the Newton's second law with the equations for the translational and rotational motion given by

$$m_i \frac{d}{dt} \mathbf{v}_i = \mathbf{f}_{\mathrm{c}i} + \mathbf{f}_{\mathrm{fp}i} + m_i \mathbf{g}, \tag{3}$$

and

$$I_i \frac{d}{dt} \boldsymbol{\omega}_i = \mathbf{T}_i, \tag{4}$$

respectively. The mass, moment of inertia, velocity, rotational velocity, force and torque of particle $i$ are denoted by $m_i$, $I_i$, $\mathbf{x_i}$, $\boldsymbol{\omega}_i$, $\mathbf{f_i}$ and $\mathbf{T_i}$, respectively. It is pointed here that bold symbols indicate vectors and $\mathbf{v_i}$ implies $[v_{xi}, v_{yi}, v_{zi}]$.

The total force acting on a particle is calculated as a sum of the total contact, the gravitational and the fluid interaction forces. The contact force ($\mathbf{f}_c$) is calculated as a sum of all the forces due to collisions with neighbouring particles. The total torque $\mathbf{T}_i$ results from a vector summation of the torque at each particle–particle contact. It is assumed that the fluid-particle interaction does not contribute to the rotational motion. A linear spring-dashpot model is employed for the contact force model with static friction between particles modelled according to the Coulomb's friction law. More details on the model can be found in [14].

*2.3. Interphase momentum transfer*

The coupling between the gas phase and particle motion is through the fluid–particle interaction $\mathbf{I}_{\mathrm{f}}$ in the gas momentum equation and $\mathbf{f}_{\mathrm{fp}i}$ in the particle equation of motion, for which following equation is used.

$$\mathbf{f}_{\mathrm{fp}i} = -V_{\mathrm{p}i}\boldsymbol{\nabla} p + \frac{\beta_i V_{\mathrm{p}i}}{\phi}\left(\mathbf{u}_{\mathrm{f}i} - \mathbf{v}_i\right), \tag{5}$$

where $V_{\mathrm{p}i}$ is the volume of particle $i$, $\phi = 1 - \epsilon$ is the solid volume fraction of the cell containing particle $i$, $\mathbf{u}_{\mathrm{f}i}$ is the fluid velocity extrapolated to the particle $i$ position and $\beta_i$ is the drag coefficient which is dependent on the drag model closures discussed below. Since the focus of this study is gas-solid fluidization, certain hydrodynamic forces dependent on fluid density and viscosity have been neglected. These include virtual mass and lift forces [2]. The total interaction $\mathbf{I}_f$ in a fluid cell is calculated by adding all particle–fluid interaction forces in the cell as

$$\mathbf{I}_f = \frac{1}{V_{\mathrm{cell}}}\sum_{i=1}^{n} \mathbf{f}_{\mathrm{fp}i} W_i, \tag{6}$$

where $V_{\mathrm{cell}}$ is the volume of the fluid cell and $W$ is the weighting function accounting for the contribution of a particle, which can be a Box-car or a Gaussian function [11].

*2.3.1. Drag model closures*

Drag models correlations were traditionally deduced from experiments on fixed bed or sedimentation [15, 16], and recently derived from resolved direct numerical simulations [17, 18, 19]. The drag coefficient in Eq. 5 can be written as

$$\beta = 18\mu\phi(1-\phi)\frac{F}{d^2}, \tag{7}$$

where $F$ is the drag force non-dimensionalized by the Stokes–Einstein drag force $(3\pi\mu d\left(\mathbf{u}_{\mathrm{f}i} - \mathbf{v}_i\right)(1-\phi))$, and $\mu$ is the fluid viscosity. This dimensionless drag force can be expressed as a function of the solid fraction ($\phi$) and the particle Reynolds number, $Re = \epsilon\rho_f d_i \left|\mathbf{u}_{\mathrm{f}i} - \mathbf{v}_{\mathrm{i}}\right|/\mu$, for a particle of diameter $d$. In this paper, we present results using two drag closures – one empirical based on experiments, often referred to as the Ergun [15] and Wen and Yu equation [16],

$$F_{\mathrm{EWY}}(\phi, Re) = \begin{cases} (1 + 0.15Re^{0.687})(1-\phi)^{-3.65} & \phi \le 0.2 \\ \frac{150}{18}\frac{\phi}{(1-\phi)^2} + \frac{1.75}{18}\frac{Re}{(1-\phi)^2} & \phi > 0.2 \end{cases}, \tag{8}$$

and the other based on recent lattice-Boltzmann simulation data [17],

$$F_{\mathrm{BT}}(\phi, Re) = \frac{10\phi}{(1-\phi)^2} + (1-\phi)^2(1+1.5\phi^{1/2}) + \frac{0.413Re}{24(1-\phi)^2}\left[\frac{(1-\phi)^{-1} + 3\phi(1-\phi) + 8.4Re^{-0.343}}{1+10^{3\phi}Re^{-(1+4\phi)/2)}}\right]. \quad (9)$$

*2.4. Numerical methods and implementation*

The locally averaged Navier-Stokes equation describing the fluid motion, is solved using OpenFOAM-1.7.1 (Open Field Operation and Manipulation) libraries, partly based on the work by Rusche [20]. The discretization employs the finite volume method on an unstructured mesh with all variables stored in cell centres. The convection and diffusion terms are discretized with a blend of central difference (with second-order accuracy) and upwind difference (with first order accuracy). The inter-phase momentum transfer term $\mathbf{I}_f$ in Eq. 2 is discretized using a semi-implicit algorithm [11] to improve the numerical stability. The implicit first-order Euler scheme is used for the time integration. The particle motion equations are solved in a particle dynamics simulator, LAMMPS (Large-scale Atomic/Molecular Massively Parallel Simulator, 2013 version ) [21]. An explicit second-order velocity Verlet algorithm is used for time integration. Readers are referred to [11] for more details about the coupling algorithms.

## 3. Simulation details and post-processing techniques

The validation study is based on a fluidized bed experiment, for which magnetic resonance (MR) measurements were carried out to obtain data for solid velocity, voidage and granular temperature [8, 7, 22] . The experiment and how it was simulated are described as follows.

*3.1. Experimental measurements and simulation details*

The fluidized bed was a pseudo 2-dimensional perspex apparatus with the dimensions of 44, 1000 and 10 mm in the width, height and depth direction, respectively. A 30 mm high granular bed consisting of kidney-shaped poppy seeds was fluidized by uniform air flowing through a porous distributor plate at the bottom. Time and spatially averaged granular temperature, solid velocity and voidage distributions were obtained using MR spectroscopy. Details of reconstructing MR data signals to obtain the data at sub-particle

size resolution can be found in [22]. The MR pixel size, which limits the spatial resolution, was $1.88^2$ mm$^2$ for granular temperature, and $0.94^2$ mm$^2$ for velocity and voidage measurements [7].

The full-scale bed was simulated with parameters for the geometry, fluid properties and contact model summarised in table 1. The fluid drag on the front and back of the bed is not included in the bed. The drag effect was not regarded as critical to the voidage and the averaged particle velocity profiles in the lateral direction, because these quantities were measured in the middle planar region of the bed (parallel to the front and back wall) in the experiments as well as in simulations [8]. The distributor plate was simulated using 4 layers of fixed particles of 1 mm diameter which covered 2 fluid cells exactly. The particle–wall interaction was modelled as either with a flat surface or with a wall consisting of solid particles, whose details will be given in section 4.3. The no-slip boundary condition was applied between fluid and all the walls. The coefficient of friction between particles and the walls was set to 0.1. DEM parameters were suggested by [8] based on values taken from the literature and employed here as the base case. A typical snap shot of the DEM-CFD simulation at a superficial velocity of 0.9 m/s can be seen in figure 1(a).

### *3.2. Post-processing of DEM data*

Post-processing of DEM data is important for the correct comparison between the experiment and the simulations. In the experiments, spatial-temporal average of the MR data was evaluated to obtain the voidage, particle velocity and granular temperature profiles in the experiments [22]. In order to have a direct comparison between DEM data and MR measurement, compatible post-processing techniques should be used. The spatial-temporal averaged solid volume fraction $\phi$ and velocity $\mathbf{V}$ at the location $\mathbf{r}$ are calculated respectively using

$$\phi(\mathbf{r}) = \frac{\pi}{6N_f} \sum_{j=1}^{N_f} \sum_{i=1}^{N_p} d_i^3 W(\mathbf{r} - \mathbf{r}_{i,j}), \tag{10}$$

and

$$\mathbf{V}(\mathbf{r}) = \frac{\sum_{j=1}^{N_f} \sum_{i=1}^{N_p} \mathbf{v}_{i,j} W(\mathbf{r} - \mathbf{r}_{i,j})}{\sum_{j=1}^{N_f} \sum_{i=1}^{N_p} W(\mathbf{r} - \mathbf{r}_{i,j})}, \tag{11}$$

where $\mathrm{d}_{i,j}$ and $v_{i,j}$ are the diameter and instantaneous velocity of a particle at a location $\mathbf{r}_i$ and a time instant $j$, respectively, $N_p$ is the number of particles

in the domain, $N_f$ is the number of time steps used in the time averaging and $W(\mathbf{r}-\mathbf{r}_i)$ is a weighting function. We used $W(\mathbf{x}) = \frac{1}{\Omega(w)}H(w-||\mathbf{x}||)$, where $H$ represents the Heavi-side function and $\Omega(w)$ is the volume of the averaging sphere of radius $w$. The averaging results were found not sensitive to the forms of the weighting function. However, the results were sensitive to the parameters of the weighting function. The calculation of solid velocity in Eq. 11 is consistent with the so-called "particle based averaging" used in [23, 24, 25], which was found to yield better agreement between DEM and experimental analysis than using the "frame based averaging" approach, in which the spatially averaged solid velocity at every time instant is averaged over time with equal weightings.

Since the MR measurements are time-averaged measurements of the mean and variance of the velocity, the MR measured variance of the velocity is a combination of both the local fluctuations about the mean velocity, and the time-averaged fluctuations of the mean velocity [7]. It is not possible to separate these contributions to granular temperature in the MR measurements. We calculate the granular temperature, consistent with that calculated in the experiments [22] as given by

$$\theta(\mathbf{r}) = \frac{1}{3}\left(\overline{V_x'V_x'} + \overline{V_y'V_y'} + \overline{V_z'V_z'}\right), \tag{12}$$

where the variance of the velocity $(\overline{V_i'V_j'})$ is defined as

$$\overline{V_i'V_j'}(\mathbf{r}) = \frac{1}{N_f}\sum_{k=1}^{N_f}\left[\overline{V}_{i,k}(\mathbf{r},t) - V_i(\mathbf{r})\right]\left[\overline{V}_{j,k}(\mathbf{r},t) - V_j(\mathbf{r})\right]. \tag{13}$$

The spatially averaged velocity $\overline{\mathbf{V}}(\mathbf{r},t)$ is calculated by

$$\overline{\mathbf{V}}(\mathbf{r},t) = \frac{\sum_{i=1}^{N_p}\mathbf{v}_i W(\mathbf{r}-\mathbf{r}_i)}{\sum_{i=1}^{N_p} W(\mathbf{r}-\mathbf{r}_i)}. \tag{14}$$

The averaged voidage, solid velocity and granular temperature are dependent on the spatial and temporal scales used for the averaging. The scales were found to be functions of number of particles, averaging time, sampling frequency and dynamics of the system. Studies have been carried out to determine the length and time scales at which the results are approximately invariant to the scales. It was found that a length scale of 2.5 times of particle diameters, a sampling frequency of 100 Hz and an averaging time of 45

seconds yield such scale invariant results. In order to make the time-averaged DEM results comparable to the experimental results, the time length used for averaging has been so determined as to make the averaged results independent of the number of instantaneous flow profiles contained. We now turn out attention to the simulation results and the comparison with the experimental results.

## 4. Results and discussions

### *4.1. Bed pressure drop analysis*

The fluidization curve for the bed was determined by simulations where the inlet velocity was linearly increased from 0.0 to 0.6 m/s. The initial packed bed porosity was around 0.328, close to experimental value of 0.33 [8]. The total pressure drop across the bed is plotted against the superficial inlet velocity in figure 2, where the pressure drop is normalised by the bed weight per unit cross sectional area and the velocity is normalised by the minimum fluidization velocity $U_{\mathrm{mf}}$ (0.3 m/s) determined in the experiments [8]. It is demonstrated that the basic fluidization phenomena can be captured correctly, i.e. that the pressure drop plateaued out at a level supporting the total weight of bed at around the $U_{\mathrm{mf}}$. The different drag models tested show little effect on the fluidization curve with the predicted $U_{\mathrm{mf}}$ values within 10 percent of the experimental value.

The absolute pressure drop, computed immediately above the distributor plate, is plotted as a function of time at the inlet velocity of 0.6 m/s (around $2U_{\mathrm{mf}}$) in figure 3a. Periodic fluctuations in the pressure drops can be observed, which are usually linked with the instabilities, such as bubbles, arising at the distributor plate. Fast Fourier Transformation (FFT) analysis of pressure drop fluctuations have been previously used to identify the fluidization regimes, e.g. bubbling or slugging [26, 27, 28]. The power spectrum obtained using the same technique is shown in figure 3b. The spectrum has multiple small peaks in the range of 0–10 Hz, and one prominent peak at around 7 Hz. These results are in a quantitative match with the pressure drop and FFT results obtained from DEM-CFD simulations of the same Geldart D particles by Boyce et al. [29], on a 3-D cylindrical fluidized bed. Furthermore, the bubble formation frequency at the distributor plate in the fluidization experiment of the same particles was found to be also around 7 Hz [29], implying a link with the large pressure fluctuations. To ensure

the dynamic process of bubble formation can be fully recorded, the data sampling frequency is chosen to be much higher at 100 Hz.

*4.2. Voidage, solid velocity and granular temperature comparison*

In this section, DEM-CFD simulation results are compared with the MR measurements of voidage, solid velocity and granular temperature for the cases with superficial fluidization velocities of 0.6 and 0.9 m/s. The base simulation case employs the drag model developed by Beetstra et al. [17], has particle–wall interaction with a frictional planar surface, and uses the parameters as specified in table 1. After undertaking parametric studies, it is found that the simulation results presented here are not sensitive to certain particle properties, such as stiffness, coefficient of restitution and sliding friction coefficient. figure 4(a) and (c) presents the 2-D contour plots of solid velocity components for the case with 0.6 m/s inlet velocity. The experimental data obtained for a $x$-$z$ cross section at the middle in the depth direction [22] is shown in figure 4(b) and (d). The vertical velocity ($V_y$) is negative close to the side walls and tends to be positive moving towards the center; the lateral velocity $V_x$ has opposite signs and symmetric to the vertical center line. Together, the time averaged velocities show that the solid particles are transported upwards in the center of the bed and downwards close to the wall, which is a robust feature in a dense bubbling bed. The DEM-CFD simulations are able to capture this solid circulation pattern qualitatively as observed in the experiments and evident from the figure 4. However, the location and magnitude of the maximum velocities observed in the experiments are not in agreement. The causes of the discrepancy are attributed to the particle sizes and are further discussed in the section 4.4 below.

The solid velocity for the case with inlet velocity of 0.9 m/s indicates a similar solid circulation pattern observed at inlet velocity of 0.6 m/s. For more quantitative comparison to the experimental results, the vertical velocities, $V_y$, at the heights of 15, 25 and 35 mm above the distributor plate are plotted across the bed width in figures 5(a), (b) and (c), respectively. Although general agreement with the experimental data is still observed for these velocity profiles, significant mismatches are found near the side walls ($x$ = 0 or 44 mm) and towards the middle section of the bed. The simulation velocities near the walls are consistently higher (more negative) than the experimental values, i.e., particles move downwards faster in the simulation, independently of the bed heights. The difference in dynamics

adjacent to the walls is also reflected in the granular temperature profiles as shown in figure 6. Such discrepancies at the wall have been investigated and attributed to the particle–wall interaction models used in the simulation, discussed later in the section 4.3. The experimental data suggests that the granular temperature decreases considerably toward the walls from the central region (around $x = 22$ mm), whereas the simulation results show an opposite trend of increasing granular temperature for all three profiles. This discrepancy in granular temperature suggests that velocity fluctuation is a more sensitive measure to reveal the dynamic state than the mean velocity for which only quantitative difference was observed. The simulation predicts higher granular temperature, indicating larger velocity fluctuations than in the experiments around the walls.

The simulation over-predicts (under-predicts) the velocity in the central region at the height of 15 mm (35mm) although has good match at the height of 25 mm. The time averaged solid fraction contours are plotted in figure 7(a), shows a gulf-like pattern with higher voidage (lower solid fraction and more dilute) in the middle of the bed at heights around 25-35 mm above the distributor plate, which was also reported by experimental finding from [22]. A lower voidage (higher solid fraction and denser) is also seen at the regions close to the walls in accordance with the experimental observations [22]. This general variation can also be seen from the voidage profile at the heights of height 16.4 (figure 7(b)) and 31.4 mm (figure 7(c)). The voidage near the walls at 31.4 mm is over-predicted by 40 percent, whereas a good match is obtained at 16.4 mm. These mismatches are intricately related to the inability of the model to capture the bed expansion correctly. The velocity contour plots in figure 4 suggests that model is not able to capture the height of maximum vertical velocity contour from the distributor plate. Effect of particle size will be addressed in the later section 4.4 to account for discrepancies for bed expansion and velocity variation along the bed height.

### *4.3. Wall boundary effect on solid velocity and voidage*

The comparison in the previous section indicated that the particle motion is retarded more in the experiments than in the simulation near the walls. The fluid–wall interaction could form a viscous layer in the near-wall region and indirectly slow down the particle dynamics. Recent direct numerical simulation (DNS) [30] found that wall friction affect the fluid flow only within one particle diameter from the wall. Furthermore, the pressure drops predicted by the Beetstra drag model were very close to the DNS results

outside of this one-diameter zone. The fluid–wall interaction thus seems unlikely to account for the solid velocity discrepancy observed in the 5-diameter boundary layer. Fluid-wall boundary effect was further tested by changing the boundary condition from the no-slip to the full-slip one, which should exert a larger effect beyond the one-diameter zone since the current simulation employs a fluid cell of about 3 particle diameters. No discernible effect was found on the solid velocity, which corroborates the point that the fluid–wall effect is not significant in determining the solid velocity around the walls.

We now focus on the particle–wall interaction. In the base simulation case, particles interact with wall via the same force model as the particle–particle interaction while taking the wall being a flat surface with Coulomb friction (refer to section 2.2. The coefficient of friction was varied from 0.1 (low friction) to 1 (highly frictional) and the wall slip velocity was not reduced significantly, indicating the wall resistance offered in the classic Coloumb friction model is not sufficient to account for the discrepancy observed in the wall slip velocity. Previous works in dry granular flows [31, 32, 33] employed static particles at the inner side of the walls, with the particle diameters in a similar range to the bulk particle sizes to provide higher effective wall friction than the flat wall model under the same flow condition and reduce the wall slip velocity as the wall-particle size increases.

We employ a similar approach: the wall surface was modeled as a vertical row of fixed spherical particles. The particles forming the walls are kept stationary by setting their velocities to zero every time step. The wall particles are arranged in a regular lattice with no spacing or overlap between them and located at both sidewall boundaries of $x = 0$ and 44 mm (figure 1(b)). Since the pattern and spacing are fixed, the particle diameter is the only variable used to tune the frictional effect of the walls. It should be noted that particle–wall boundaries are employed only for the DEM calculation while the fluid–wall boundary condition remains as flat walls with no slip. Figure 8(a) compares the effect of particle-walls on the solid velocity for the profile at the height of 25 mm with the base simulation and the experimental results. Similar results for solid velocities have been found for other heights at 15 and 35 mm, but not shown here. It can be seen that the magnitudes of the velocities in the wall boundary layers are reduced by 40–60% for the particle wall configuration. Figure 8(b) shows the zoomed-in profiles in the near wall region at higher spatial resolution. It can also be seen that increasing the wall particle diameter results in a greater reduction of solid wall-slip velocity in the wall boundary layers. Such walls with particles of diameter

less $0.1d$ produce simular results to the flat wall, and not shown here for clarity. These trends are consistent with the previous findings for dry granular flows [31, 32, 33], but demonstrates that the particle–wall interaction dominates the dynamics in this dense gas-solid fluidization situation. The particle-wall does affect the velocities beyond the boundary layers, albeit to a much smaller extent, which also increases with larger wall particles. At the diameter equal to $2d$, there are appreciable differences from the experimental values in the central region. In addition, the predicted granular temperature trend reverses from increasing to decreasing toward the walls when the particle-wall boundary is employed (figure 6), producing excellent match both in trend and in magnitude with the experimental measurement. As the detailed wall friction condition is not known from the available experiment data, however, we are limited to qualitative comparison of the effect of such walls, rather than to pin down if the same magnitude of wall friction led to the observed wall slip velocity and granular temperature profiles in the experiments.

Examining the particle packing structure more closely, oscillations are found in the particle (igure 9(a)) and voidage (figure 9(b)) distributions close to the walls and converge to the bulk values after about 5 particle diameters. The histograms are plotted by tabulating frequency of particles present at a particular distance $r/d$. The particle positions are counted in a region 20–30 mm above distributor plate over 40 seconds of simulation at a high sampling rate of 200 Hz. A distribution function of the particle positions is plotted by normalizing the histogram plot by area under the curve. The zero $x$-coordinate in figure 9 is set to the position of either the flat surface or the center of wall particles. Such oscillations in voidage have been reported for the particle packing probed by NMR spectroscopy [34]. The particle wall leads to important difference in the distributions, particularly for those within 0.5 diameter from the wall. Particles are all excluded from the flat wall by their own volumes and have the highest probability located 0.5 diameter away, where the voidage is correspondingly lowest. This dense layer of particles slide along the wall. On the contrary, there are more particles distributed within the $0.5d$ region when the particle wall is present, which contributes to greater resistance to the particle flow.

The wall boundary analysis shows that the particle–wall interaction dominates the particle dynamics in the boundary layers of about 5 particle diameters. The classic Coloumbic friction in the planar wall could not capture the granular resistance near the wall.

*4.4. Particle size effects*

Apart from the dynamics close to the walls, mismatch has also been observed in the middle region especially for the heights at 15 and 35 mm, for example see figure 5. This type of mismatch is related to how bed dynamics varies along the bed height direction, which is thought to be sensitive to the particle shape and size.

Kidney-shaped poppy seeds, which naturally have variations in size, were used in these MR fluidization experiments [8]. Such size distributions have been neglected in the simulations, for which mono-disperse sphere with diameter of 1.2 mm were used as described in section 3. Without performing extensive parametric studies using poly-disperse non-spherical particles, we used a set of simplified simulations to probe the sensitivity to particle sizes. We performed simulations of mono-disperse spheres at different diameters, namely 1.1 and 1.3 mm, maintaining roughly the same initial bed height and weight as those of the 1.2 mm diameter particles. The simulated minimum fluidization velocity was thus kept in the range of 0.28–0.32 m/s, close to the experimental value, 0.3 m/s. The variation of velocity $V_y$ along bed height is plotted in figure 10 for the three different particle diameters at a fluidization velocity equal to 0.6 m/s. The solid velocity profile is calculated at $x =$ 22 mm with bin size equal to 2.5 d in the $x$ and $y$ direction and averaged over whole depth ($z$) direction. These profiles are significantly different from each other with the maximum velocity magnitude increased by 50% for a 18% decrease in the particle diameter. Such a change in magnitude is close to the mismatch between the base simulation and the experimental results (refer to the contour plots in figure 4). The velocity is higher for smaller particles at all the positions below 40 mm, above which negative velocities for 1.1 and 1.2 mm particles appear, indicating higher bed expansion. This velocity variation combined with the segregation tendency of a fluidized bed could qualitatively explain the mismatches observed in the middle region at the heights of 15 and 35 mm. Imagining the poppy seeds have larger and smaller particles, the former would tend to concentrate toward the lower part of the bed and the latter to the upper. As we choose to use particles of a mean size in the simulation, it would over-predict solid velocity in the lower and under-predict it in the upper part, the same as observed in figure 5. The shape effects of the particles are rather difficult to quantify in the current DEM-CFD framework.

## 5. Conclusions

We have presented validation and model sensitivity studies for a DEM-CFD methodology and its numerical implementation in a computer code. The methodology couples the spatially averaged Navier-Stokes equation for fluid and the Newtonian motion equations for individual particles. The code has been used to simulate the fluidization experiments, for which MR measurements have been performed by other researchers. It has been shown that the simulation is able to accurately capture the minimum fluidization velocity, pressure drop fluctuations and its major frequency measured in the experiments. Further comparison of the spatial-temporally averaged solid velocity shows that the solid circulation pattern can also be reproduced qualitatively, but robustly independent of the model parameters. Quantitative discrepancies, however exist, in the spatial-temporally averaged voidage, solid velocity and granular temperature profiles, most noticeably in the near wall regions, and in the middle at the upper or lower bed. The level of the differences is largely in line with that previously discovered by other DEM-CFD simulations.

Although such discrepancies are intricately related to various model simplifications and may not be fully addressed in the DEM-CFD framework, it is important to identify how the physical models employed affect the simulation predictions and how sensitive these effects to model parameters. To this end, we have found that the particle–wall interaction dominates the particle dynamics over the fluid–wall interaction in a wall boundary layer of about 5 particle diameter wide. Using a solid wall consisting of particles provides more resistance to the particle motion than using a smooth frictional wall, reducing the mean and variance of particle velocities and leading to closer agreement with the experimental data. This finding shows the importance of the wall boundary for DEM-CFD simulation and leads to the interesting question of how to model such wall boundary layers in a continuum two-fluid model framework, for which proper boundary conditions are essential for correct prediction of large-scale flow behaviour. The data here suggests that models of effective wall boundary conditions for solid velocity and granular temperature in a two-fluid model could be constructed using the particle dynamics data in such boundary layers.

The bed expansion and dynamics have been found to be sensitive to the particle size. Smaller particles have higher vertical velocities throughout the bed, which implies that size segregation could be a factor contributing to the

over-(under-)prediction of velocities at the lower (upper) parts of the bed. These findings also point to some problems warranting further studies. It would be interesting to conduct DEM-CFD simulations using spherical particles with a size distribution which has the mean of 1.2 mm and a small variance to test if such size distributions contribute to the velocity discrepancies observed in the lower and upper bed. In the same spirit, DEM-CFD simulations of non-spherical particles together with modified drag force models could quantify the effect of the particle–particle interaction in this condition.

## Acknowledgements

The work was supported by the European Commission Framework Programme 7 through the Marie Curie Initial Training Network, PARDEM (www.pardem.eu). The authors would also like to acknowledge Dr. Heng Xiao for his help on the code used in the work. All data used within this publication can be accessed at http://dx.doi.org/xxxxx.

## References

[1] M. A. van der Hoef, M. van Sint Annaland, N. G. Deen, J. A. M. Kuipers, Numerical simulation of dense gas-solid fluidized beds: A multiscale modeling strategy, Annu. Rev. Fluid Mech. 40 (2008) 47–70.

[2] H. P. Zhu, Z. Y. Zhou, R. Y. Yang, A. B. Yu, Discrete particle simulation of particulate systems: theoretical developments, Chemical Engineering Science 62 (13) (2007) 3378–3396.

[3] N. G. Deen, M. Van Sint Annaland, M. A. van der Hoef, J. A. M. Kuipers, Review of discrete particle modeling of fluidized beds, Chemical Engineering Science 62 (1) (2007) 28–44.

[4] Y. Q. Feng, A. B. Yu, Microdynamic modelling and analysis of the mixing and segregation of binary mixtures of particles in gas fluidization, Chemical Engineering Science 62 (1) (2007) 256–268.

[5] J. M. Link, N. G. Deen, J. A. M. Kuipers, X. Fan, A. Ingram, D. J. Parker, J. Wood, J. P. K. Seville, PEPT and discrete particle simulation study of spout-fluid bed regimes, AIChE Journal 54 (5) (2008) 1189–1202.

[6] C. R. Müller, J. F. Davidson, J. S. Dennis, P. S. Fennell, L. F. Gladden, A. N. Hayhurst, M. D. Mantle, A. C. Rees, A. J. Sederman, Real-time measurement of bubbling phenomena in a three-dimensional gas-fluidized bed using ultrafast magnetic resonance imaging, Physical review letters 96 (15) (2006) 154504.

[7] C. R. Müller, D. J. Holland, A. J. Sederman, S. A. Scott, J. S. Dennis, L. F. Gladden, Granular temperature: comparison of magnetic resonance measurements with discrete element model simulations, Powder Technology 184 (2) (2008) 241–253.

[8] C. R. Müller, S. A. Scott, D. J. Holland, B. C. Clarke, A. J. Sederman, J. S. Dennis, L. F. Gladden, Validation of a discrete element model using magnetic resonance measurements, Particuology 7 (4) (2009) 297–306.

[9] T. Li, R. Garg, J. Galvin, S. Pannala, Open-source mfix-dem software for gas-solids flows: Part II — validation studies, Powder Technology 220 (2012) 138–150.

[10] D. Gidaspow, Multiphase flow and fluidization: continuum and kinetic theory descriptions, Academic press, 1994.

[11] H. Xiao, J. Sun, Algorithms in a Robust Hybrid CFD-DEM Solver for Particle-Laden Flows., Communications in Computational Physics 9 (2) (2011) 297.

[12] T. B. Anderson, R. Jackson, Fluid mechanical description of fluidized beds. Equations of motion, Industrial & Engineering Chemistry Fundamentals 6 (4) (1967) 527–539.

[13] R. Jackson, Locally averaged equations of motion for a mixture of identical spherical particles and a Newtonian fluid, Chemical Engineering Science 52 (15) (1997) 2457–2469.

[14] J. Sun, F. Battaglia, S. Subramaniam, Hybrid Two-Fluid DEM Simulation of Gas-Solid Fluidized Beds, Journal of Fluid Engineering 129 (11) (2007) 1394–1403.

[15] S. Ergun, Fluid flow through packed columns, Chem. Eng. Prog. 48.

[16] C. Y. Wen, Y. H. Yu, A generalized method for predicting the minimum fluidization velocity, AIChE Journal 12 (3) (1966) 610–612.

[17] R. Beetstra, M. A. van der Hoef, J. A. M. Kuipers, Drag force of intermediate Reynolds number flow past mono-and bidisperse arrays of spheres, AIChE Journal 53 (2) (2007) 489–501.

[18] M. A. van der Hoef, R. Beetstra, J. A. M. Kuipers, Lattice-Boltzmann simulations of low-Reynolds-number flow past mono-and bidisperse arrays of spheres: results for the permeability and drag force, J. Fluid Mech 528 (2005) 233–254.

[19] X. Yin, S. Sundaresan, Drag Law for Bidisperse Gas- Solid Suspensions Containing Equally Sized Spheres, Industrial & Engineering Chemistry Research 48 (1) (2008) 227–241.

[20] H. Rusche, Computational fluid dynamics of dispersed two-phase flows at high phase fractions, Ph.D. thesis, Imperial College London (University of London) (2003).

[21] S. Plimpton, Fast parallel algorithms for short-range molecular dynamics, Journal of Computational Physics 117 (1) (1995) 1–19.

[22] D. J. Holland, C. R. Müller, J. S. Dennis, L. F. Gladden, A. J. Sederman, Spatially resolved measurement of anisotropic granular temperature in gas-fluidized beds, Powder Technology 182 (2) (2008) 171–181.

[23] C. M. Boyce, D. J. Holland, S. A. Scott, J. S. Dennis, Adapting data processing to compare model and experiment accurately: a discrete element model and magnetic resonance measurements of a 3d cylindrical fluidized bed, Industrial & engineering chemistry research 52 (50) (2013) 18085–18094.

[24] T. Weinhart, A. R. Thornton, S. Luding, O. Bokhove, From discrete particles to continuum fields near a boundary, Granular Matter 14 (2) (2012) 289–294.

[25] C. Labra, J. Ooi, J. Sun, Spatial and temporal coarse-graining for dem analysis, in: POWDERS AND GRAINS 2013: Proceedings of the 7th International Conference on Micromechanics of Granular Media, Vol. 1542, AIP Publishing, 2013, pp. 1258–1261.

[26] D. Bai, J. R. Grace, J.-X. Zhu, Characterization of gas fluidized beds of group c, a and b particles based on pressure fluctuations, The Canadian Journal of Chemical Engineering 77 (2) (1999) 319–324.

[27] C. A. S. Felipe, S. Rocha, Time series analysis of pressure fluctuation in gas-solid fluidized beds, Brazilian Journal of Chemical Engineering 21 (3) (2004) 497–507.

[28] H. Kage, M. Agari, H. Ogura, Y. Matsuno, Frequency analysis of pressure fluctuation in fluidized bed plenum and its confidence limit for detection of various modes of fluidization, Advanced Powder Technology 11 (4) (2000) 459–475.

[29] C. M. Boyce, J. F. Davidson, D. J. Holland, S. A. Scott, J. S. Dennis, The origin of pressure oscillations in slugging fluidized beds: Comparison of experimental results from magnetic resonance imaging with a discrete element model, Chemical Engineering Science 116 (2014) 611–622.

[30] T. Tsuji, E. Narita, T. Tanaka, Effect of a wall on flow with dense particles, Advanced Powder Technology 24 (2) (2013) 565–574.

[31] Z. Shojaaee, J.-N. Roux, F. Chevoir, D. E. Wolf, Shear flow of dense granular materials near smooth walls. i. shear localization and constitutive laws in the boundary region, Physical Review E 86 (1) (2012) 011301.

[32] N. Estrada, A. Taboada, F. Radjai, Shear strength and force transmission in granular media with rolling resistance, Physical Review E 78 (2) (2008) 021301.

[33] T. Weinhart, A. Thornton, S. Luding, O. Bokhove, Closure relations for shallow granular flows from particle simulations 14 (4) (2012) 531–552.

[34] A. Sederman, P. Alexander, L. Gladden, Structure of packed beds probed by magnetic resonance imaging, Powder Technology 117 (3) (2001) 255–269.

**List of Figures**

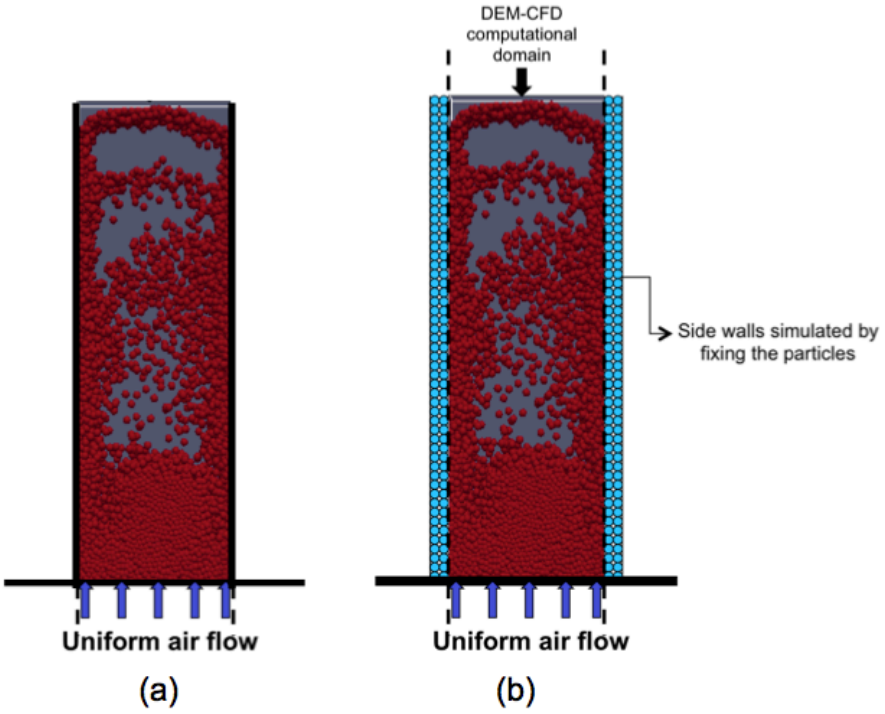


Figure 1: A typical snapshot of DEM–CFD simulation of a gas-solid fluidized bed with particle diameter of 1.2 mm and density of 1000 kg/m$^3$ at the inlet velocity of 0.9 m/s. (a) Base case, flat side walls (b) Simulation domain with particle-wall boundaries.

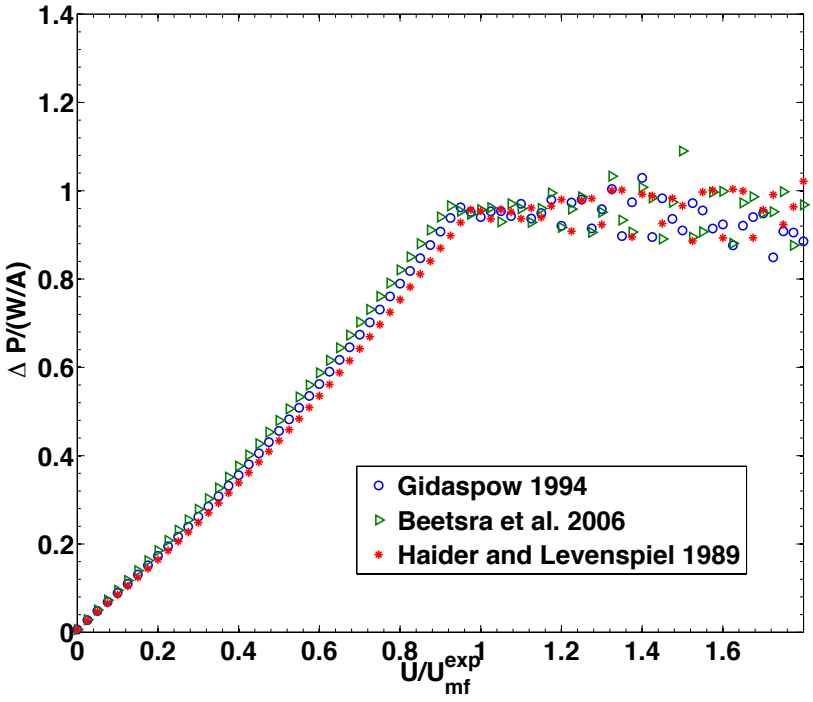


Figure 2: Pressure drop ($\Delta P$) across the bed (normalised with the bed weight, $W$ divided by bed cross section area, $A$) plotted against the fluid inlet velocity (normalised by experimental minimum fluidization velocity $U_{\mathrm{mf}}^{\mathrm{exp}} = 0.3$ m/s) for different drag models.

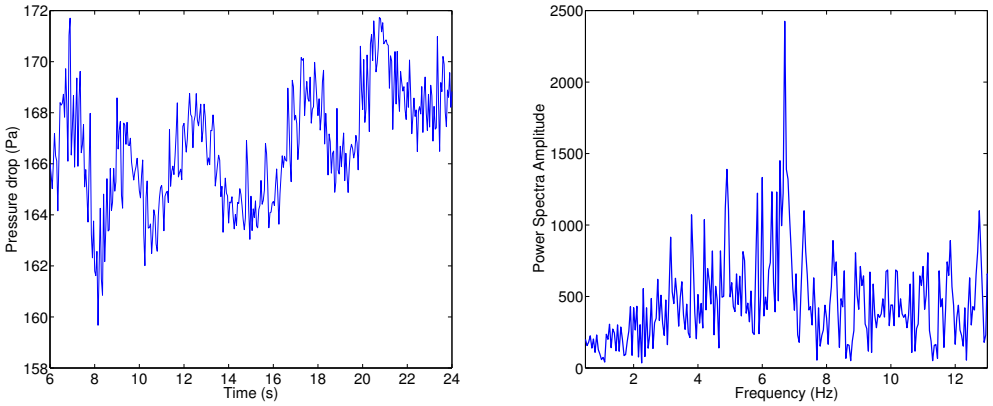


(a) (b)

Figure 3: (a) Pressure drop across the bed plotted against time at the fluidization velocity of 0.6 m/s (b) Power-spectra obtained from FFT of pressure drop data. The dominant peak around 7 Hz indicates a slugging frequency around 7 Hz.

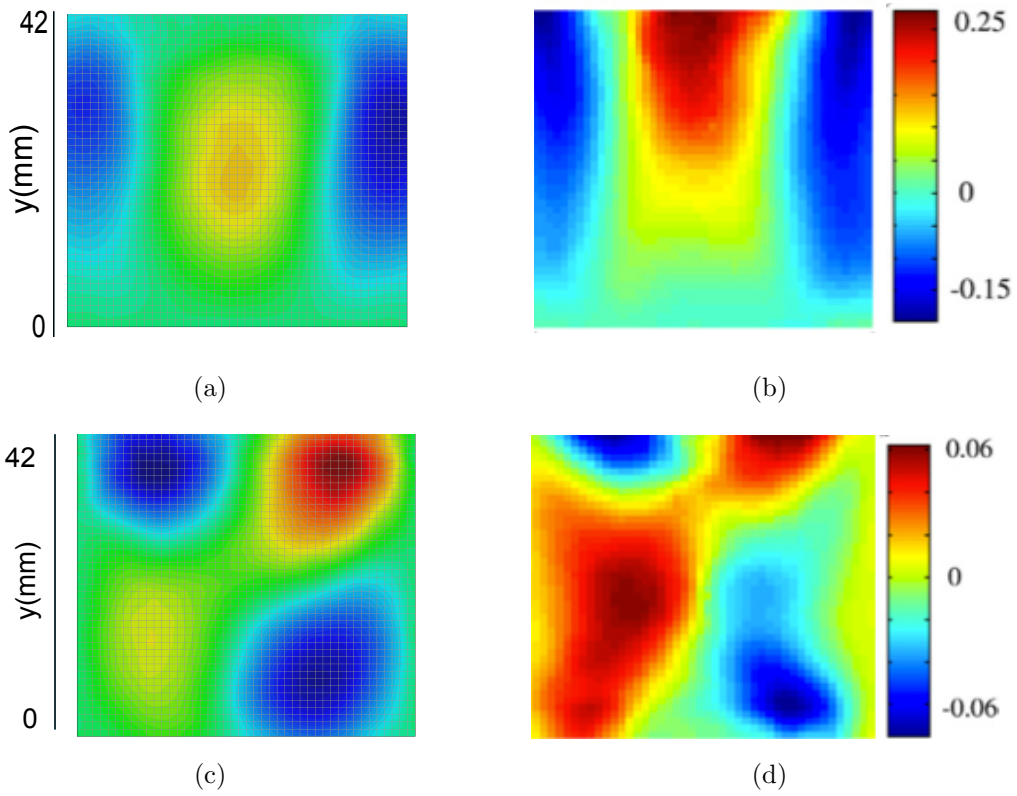


Figure 4: 2D Contour plots of solid velocity components (a) $V_y$ and (c) $V_x$ obtained from DEM-CFD simulations compared with the corresponding MR measurements in (b) and d (reproduced from [22]) for the case with the superficial fluidization velocity of 0.6 m/s.

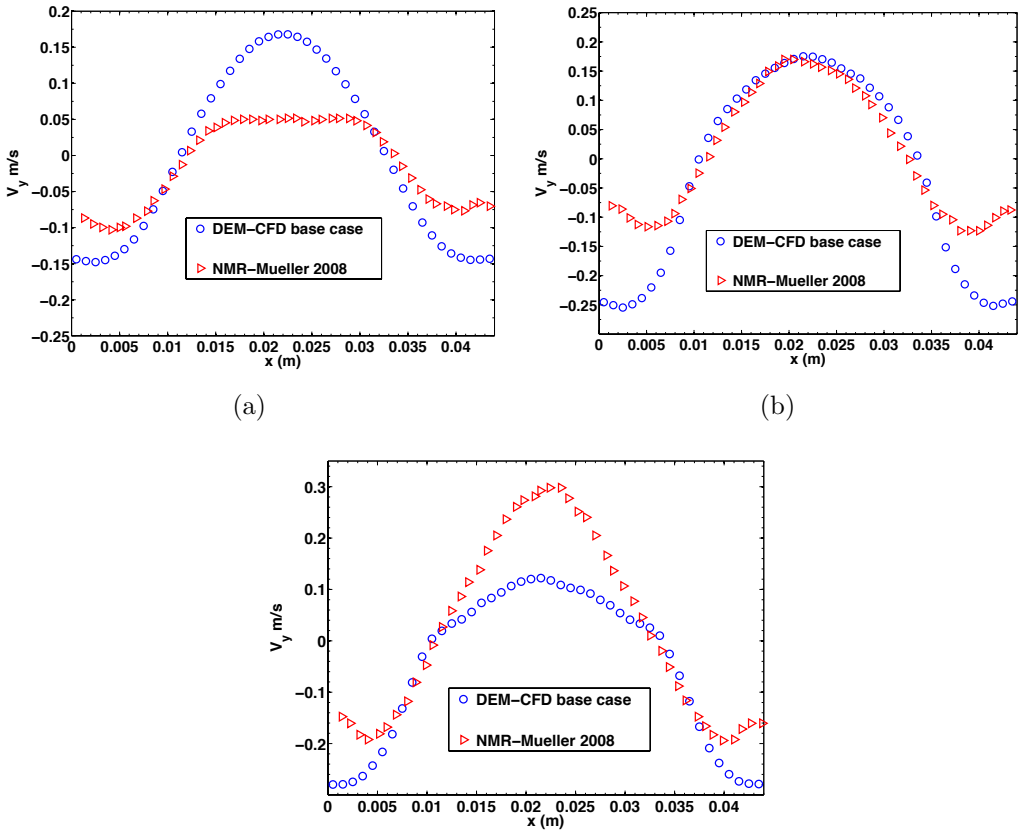


Figure 5: Vertical velocity profiles at the heights of (a) 15 mm, (b) 25 mm and (c) 35 mm above the distributor plate at the fluidization velocity of 0.9 m/s, comparing the simulation with the experimental results by Müller et al. [7].

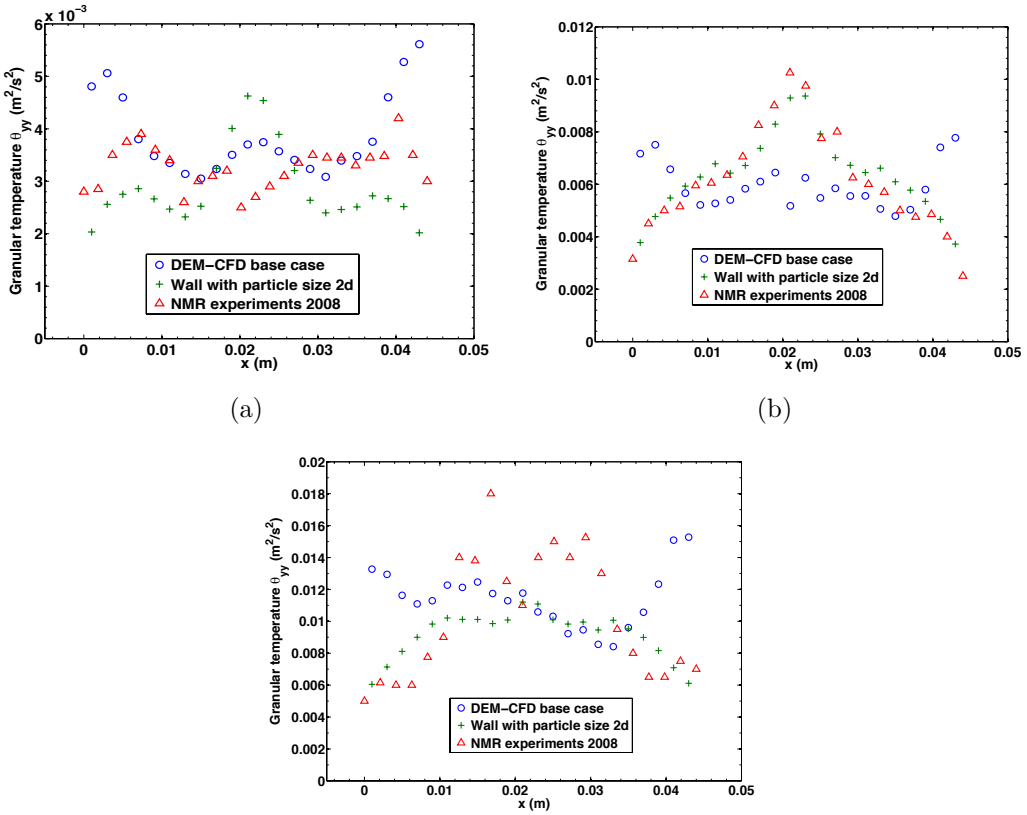


Figure 6: Granular temperature (the *yy*-component) profiles at the heights of (a) 7.5 mm, (b) 20 mm and (c) 35 mm above the distributor plate at the fluidization velocity of 0.9 m/s, comparing the simulation with the experimental results by Müller et al. [7].

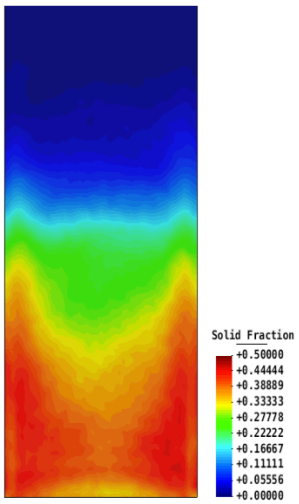


(a)

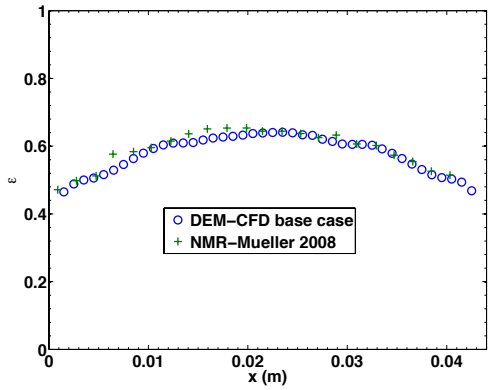


(b)

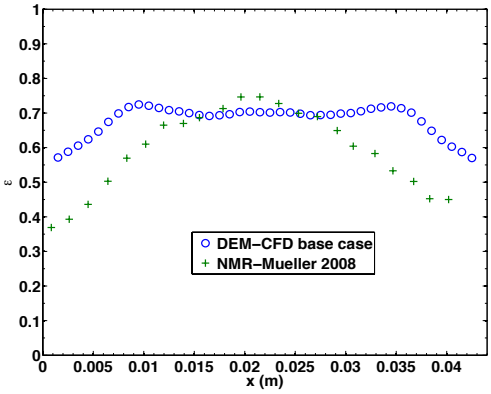


(c)

Figure 7: (a) 2D solid fraction contour obtained from the DEM-CFD simulation. Voidage profiles at the heights of (b) 16.4 mm and (c) 31.2 mm above distributor plate at the fluidization velocity of 0.9 m/s, comparing the simulation with the experimental results by Müller et al. [7].

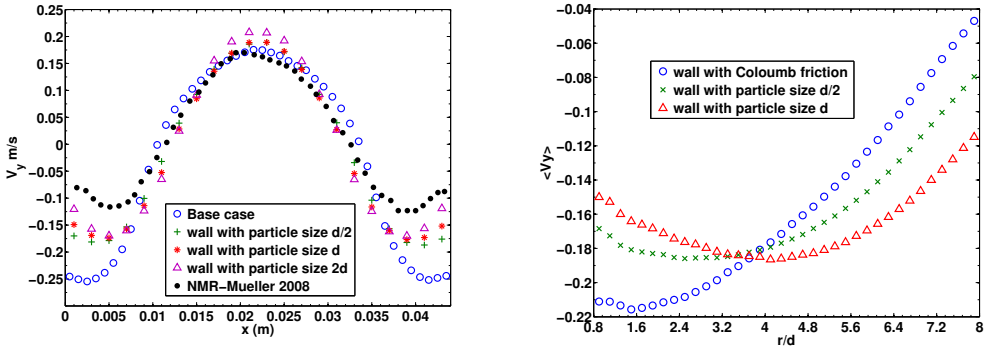


(a) (b)

Figure 8: (a) Vertical velocity profiles at the height of 25 mm at the fluidization velocity of 0.9 m/s obtained from simulations with rough walls modelled using fixed particle of different diameters, comparing to the base simulation case and the experimental results. (b) Zoomed-in view of the averaged particle velocity around the walls, post-processed with higher time and spatial resolution.

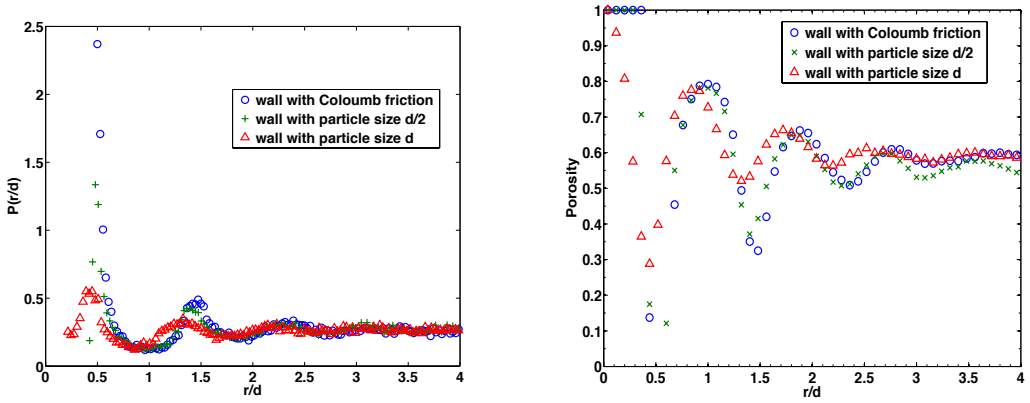


(a) (b)

Figure 9: (a) Distribution function of particle locations and (b) time averaged voidage plotted against the distance from the wall (normalised with the particle diameter) for different particle-wall conditions.

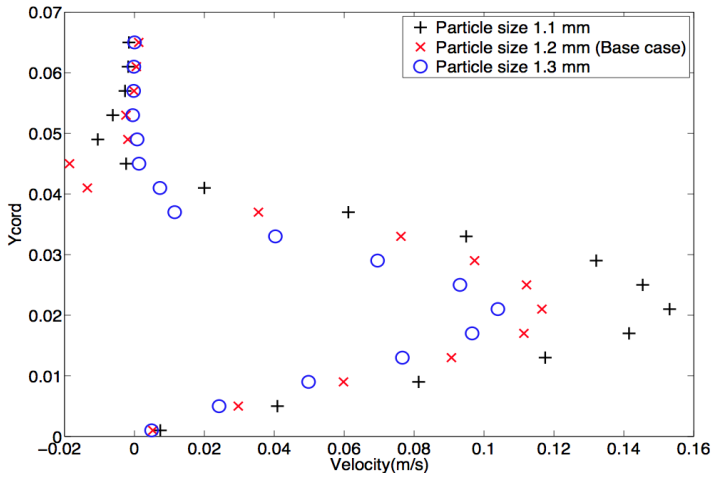


Figure 10: Variation of the vertical velocity along the bed height for the beds of particles with diameters equal to 1.1,1.2 and 1.3 mm respectively at the fluidization velocity of 0.6 m/s.

**List of Tables**

| **DEM Parameter** | **Value** |
|---|---|
| Number of Particles | 9240 |
| Diameter, $mm$ | 1.2 |
| Sphericity | 1 |
| Particle Density, $\rho$ (kg/m$^3$) | 1000 |
| Spring Stiffness, $k$ (N/m) | 200 |
| Coefficient of resitution, $e$ (N/m) | 0.98 |
| Inter-particle friction coefficient, $\mu$ (N/m) | 0.1 |
| Particle-wall friction coefficient, $\mu$ (N/m) | 0.1 |
| **Gas Phase** | |
| Gas density, $\rho_f$ (kg/m$^3$) | 1.225 |
| Gas viscosity, $\mu_f$ (Pa $\cdot$ s) | 1.8e-5 |
| Inlet velocity, $v_f$ (m/s) | 0.6,0.9 |
| Wall boundary condition | No-slip |
| Inlet boundary condition | Uniform inflow |
| Outlet boundary condition | Pressure outlet, $10^5$ Pa |
| **Geometry** | |
| Bed width ($x$), m | 0.044 |
| Bed height ($y$), m | 0.12 |
| Bed thickness ($z$), m | 0.01 |
| Discretization length ($\Delta x$), m | 0.004 |
| Discretization length ($\Delta y$), m | 0.003 |
| Discretization length ($\Delta z$), m | 0.01 |

Table 1: Domain size and DEM-CFD simulation parameters